

## Quasi-Biennial and Subbiennial Variations of Stratospheric Trace Constituents Derived from HALOE Observations

TIMOTHY J. DUNKERTON

*Northwest Research Associates, Inc., Bellevue, Washington*

(Manuscript received 3 June 1999, in final form 27 April 2000)

### ABSTRACT

Interannual variability of trace constituents in the stratosphere is examined using methane, water vapor, and ozone data from the Halogen Occultation Experiment aboard the *Upper Atmosphere Research Satellite* in 1992–99. Application of rotated principal component analysis to the dataset reveals dominant modes of variability consisting of annual, semiannual, and quasi-biennial oscillations (QBOs), together with “subbiennial” variations evidently due to nonlinear interaction between the annual cycle and QBO. The structure of quasi-biennial variability is approximately symmetric about the equator, while subbiennial variability, with certain exceptions, is approximately antisymmetric and confined mostly to the subtropics. The vertical structure and downward propagation of the ozone QBO at the equator is described by a pair of symmetric EOFs having separate amplitude maxima in the lower and upper stratosphere. A second pair of EOFs explains the seasonal dependence of subtropical ozone anomalies. For each tracer, the subtropical anomaly is larger in the Northern Hemisphere.

A novel “phase diagram” illustrates the joint seasonal and QBO dependence of tracer anomalies. A pair of principal components are used to define the phase of the dynamical QBO. When plotted against the phase of the annual cycle, the QBO follows a diagonal trajectory with regular phase progression except for an occasional slowing of easterly shear-zone descent near 50 hPa. Tracer principal components of symmetric and antisymmetric EOFs, plotted along this trajectory, display the distinct signatures of quasi-biennial and subbiennial variation. Tracer anomalies reconstructed using an idealized representation of QBO and subbiennial harmonics display the seasonal synchronization and decadal modulation characteristic of QBO–annual cycle interaction.

### 1. Introduction

Observations of trace chemical constituents in the stratosphere and mesosphere have been obtained by the Halogen Occultation Experiment (HALOE; Russell et al. 1993) since 1991 as part of the *Upper Atmosphere Research Satellite (UARS)* mission (Reber et al. 1993). Early results from HALOE and other *UARS* instruments were discussed in a special issue of the *Journal of the Atmospheric Sciences* (15 October 1994). Today, HALOE continues to provide data of high quality. These continuing observations have made possible a more rigorous investigation of trace constituent variability and trends (Cordero et al. 1997; Luo et al. 1997; Rosenlof et al. 1997; Ruth et al. 1997; Nedoluha et al. 1998a,b; Evans et al. 1998; Jackson et al. 1998; Randel et al. 1998, 1999a,b; Siskind et al. 1998; Gray and Russell 1999). The length of HALOE record now exceeds that of the Stratospheric and Mesospheric Sounder (SAMS) that flew aboard *Nimbus-7* in 1978–83 and provided the

first view of climatological variations of long-lived tracers in the middle atmosphere (Jones and Pyle 1984; Gray and Pyle 1986; Holton and Choi 1988; Stanford et al. 1993). With HALOE data it is possible to examine interannual variability and trends in addition to climatological variations. The purpose of this paper is to discuss the interannual variability of methane, water vapor and ozone observed by HALOE. A companion paper discusses the climatological, intraseasonal, and interannual variability of stratospheric circulation in the U.K. Met. Office (UKMO) analyses (Dunkerton 2000).

Much of the variability of zonally averaged long-lived tracers in the middle atmosphere is due to advection by mean meridional circulations associated with departures from radiative equilibrium. The observed temperature and estimated radiative equilibrium temperature have a strong annual variation, as does their difference. Planetary wave transport in the winter hemisphere maintains temperatures above radiative equilibrium, implying a net radiative cooling that is largely balanced by adiabatic warming due to subsidence. Upwelling in the stratosphere near solstice is largest in the summer subtropics (Solomon et al. 1986; Dunkerton 1991). The subtropical maximum creates a “single peak” of long-lived tracers (e.g., methane) on the summer side of the

---

*Corresponding author address:* Dr. Timothy J. Dunkerton, Northwest Research Associates, Inc., P.O. Box 3027, Bellevue, WA 98009-3027.

E-mail: tim@nwra.com

equator (Jones and Pyle 1984). This is in contrast to a symmetric “double peak” observed at equinox in connection with the westerly phase of the stratopause semi-annual oscillation (SAO; Gray and Pyle 1986). In the equatorial lower stratosphere the tracer distribution is affected by the quasi-biennial oscillation (QBO; Trepte and Hitchman 1992). SAO and QBO tracer variations, like those of the annual cycle, arise primarily from mean meridional advection associated with radiative heating anomalies (Kennaugh et al. 1997; Jones et al. 1998; Randel et al. 1998; Kinnersley 1999).

These elements of tracer variability—annual cycle, SAO, and QBO—correspond to the dominant variations of mean zonal wind in stratospheric analyses (Dunkerton 2000, and references therein). Long-lived tracers, however, display a more complicated temporal variation owing to the fact that their anomalies are created, in part, by an advective or “quadratic” nonlinearity in the tracer transport equation. Quasi-biennial anomalies of mean motion, for example, act on tracer fields distorted by the seasonal cycle, and vice versa. This nonlinear interaction generates new frequencies not present in the advecting mean meridional circulation (Gray and Dunkerton 1990; Tung and Yang 1994). The combination of signals attributable to linear and nonlinear interaction may yield a tracer time series having anomalies exactly synchronized with the seasonal cycle while undergoing low-frequency modulation on the timescale of several years, that is, the time required for phase onsets of the QBO to advance through a calendar year (Gray and Dunkerton 1990). The longest record of such behavior is in column ozone (Hilsenrath and Schlesinger 1981; Hasebe 1984; Lait et al. 1989; Holton 1989; Hamilton 1989; Gray and Dunkerton 1990; Tung and Yang 1994).

Seasonal synchronization of subtropical QBO anomalies may be attributable to mean meridional advection or to another mechanism, such as the QBO modulation of planetary wave mixing, whose influence varies depending on the time of year (Hamilton 1989). This effect will create additional frequencies in the data. Coupling between the seasonal cycle and interannual variability is implicit in regression models in which the coefficients (e.g., those of the QBO) depend on the calendar month (Randel and Cobb 1994). Some evidence that eddy transport is important is seen in (i) the observed steep gradients or apparent “transport barriers” at the edges of the polar vortex and surf zone (King et al. 1991; Murphy et al. 1993; Randel et al. 1994), (ii) images of breaking planetary waves in tracer maps (Leovy et al. 1985; Dunkerton and O’Sullivan 1996), and (iii) an observed in-phase relationship between tracer concentration and residual mean vertical advection in the tropical upper stratosphere (Randel et al. 1998).

In contrast to column ozone, which has an extensive history of ground-based measurements, the latitude–height structure of tracers in the middle atmosphere is less well known. In particular, little is known about how tracers respond in situ to the combination of QBO and

seasonal cycle. Prior to 1991, only a limited amount of satellite data were available for QBO tracer studies. In addition to the SAMS investigations cited above, Sun and Leovy (1990) isolated a QBO signature in the upper stratosphere using solar backscatter ultraviolet ozone data. The vertical structure of the ozone QBO was described using a few years of Stratospheric Aerosol and Gas Experiment (SAGE II) data by Zawodny and McCormick (1991). Since the launch of *UARS*, satellite observation of long-lived tracers has become routine. During the *UARS* observing period the QBO has maintained a period slightly in excess of 2 yr, allowing the definition of an approximate “tracer QBO” as a year-to-year difference in HALOE data (T. Dunkerton et al. 2000, in preparation).

In recent years the techniques of principal component analysis (PCA) and singular value decomposition (SVD) have proven useful in the investigation of stratospheric circulation and trace constituent behavior (Dunkerton 2000). For example, Randel and Wu (1996) and Randel et al. (1998) performed SVD between Singapore rawinsonde data (containing the QBO) and SAGE II and HALOE observations, respectively. As shown herein, application of rotated PCA to the HALOE dataset yields a compact description of observed tracer variability and provides insight into tracer behavior and the existence of new frequencies in the time series of rotated principal components. The analysis to follow will use rotated PCA instead of unrotated SVD and will focus exclusively on the HALOE observations equatorward of 52°.

## 2. Data analysis

HALOE sounding data (version 19) were binned into monthly means on a latitude–height grid, combining sunrise and sunset observations. The specified latitudinal resolution is 4°, with 34 levels evenly spaced in log pressure from 215 to 0.316 hPa. Only stratospheric levels were used in the analysis. Bad data points were removed manually. For climatological fields, a minimum of 4 yr was required at each grid point. Missing data were filled by a simple procedure in which values at the boundaries of “good-data” regions in the time–latitude plane were diffused into the interior of “missing-data” regions while being relaxed to climatology. This procedure was applied only where climatological values were defined in accord with the specified threshold. The method is a generalization of that used by Oort (1983) to fill data gaps, and avoids the problem of data discontinuities created by straight substitution of climatological values. Application of quality control and filling of missing values were necessary mainly below 46 hPa, prior to 1993, owing to Pinatubo aerosol early in the record. Since data at upper levels were unaffected by aerosol, it was desirable to retain, rather than to discard, these early data in order to maximize the length of record for EOF analysis. The data used extend from January 1992 through December 1999. EOFs were de-

finned within  $52^\circ$  of the equator so that the time series at each grid point would be entirely free of gaps.

Varimax rotation of EOFs and their associated principal component time series was performed as in Dunkerton's (2000) analysis of UKMO data. The linear trend in HALOE data was removed prior to EOF analysis. Unfortunately, perhaps owing to the more complicated or noisier quality of HALOE data, relative to UKMO, it proved impossible to cleanly separate climatological and interannual variations in EOFs obtained from the original data. Therefore, we analyze climatological and interannual variations separately. In this case the climatology was defined in the usual way as the average of all Januaries, Februaries, etc.; and the interannual variation as the residual after subtraction of the climatology. Details of climatological variations, described in an earlier version of this paper, are available from the author. The resulting decomposition of variance is not optimum in a statistical sense, but provides a more meaningful description of phenomena responsible for tracer variability, and hopefully will better approximate the decomposition of variance obtained with a much longer record.

A preliminary analysis using 6 yr of version 18 HALOE data gave results nearly identical to those reported herein, save for the trends of methane and water vapor, which were somewhat larger in the 6-yr period ending in 1997. Also, time-mean values of methane and water vapor were slightly larger in the lowermost equatorial stratosphere, by about 0.1 and 0.2 ppmv, respectively. For the purpose of anomaly analysis, differences between the two datasets were negligible.

### 3. Principal components

#### *a. Tracer variance*

Standard deviations of climatological and residual (mostly interannual) variability of methane, water vapor, and ozone are shown in Figs. 1a–f. The primary maximum of methane climatological variance (Fig. 1a) is south of the equator, in the upper stratosphere (Randel et al. 1998). This asymmetry suggests that the Brewer–Dobson circulation is stronger in northern winter than in southern winter, owing to stronger planetary wave activity, as also implied by the seasonal variation of the SAO (Delisi and Dunkerton 1988). The residual variance of methane (Fig. 1b), due primarily to interannual variations, occupies a smaller latitude range and is asymmetric about the equator in the middle stratosphere, with larger values in the Northern Hemisphere. The shape of the pattern near 10 hPa is symmetric about the equator, but maximum values are considerably larger in the Northern Hemisphere. It is unclear whether this asymmetry of amplitude is a permanent feature or the result of inadequate sampling. Caution is needed because the QBO onset has not yet advanced through an entire calendar year in the *UARS* observing period, as

discussed below. Additional years of data are needed in order to sample equally all combinations of QBO and seasonal cycle. The regions of maximum interannual variance correspond roughly to the regions of maximum gradient of time-mean methane in the latitude–height plane (not shown). The absence of equatorial variance below 10 hPa is remarkable since the time-mean gradient, while small, is nonzero here.

The climatological variability of water vapor (Fig. 1c) mimics that of methane at upper levels with about twice the magnitude, but includes one or two new features at lower levels. There is a broad “plume” of variance extending upward from the tropical tropopause and a sharp local maximum at the tropopause in the northern subtropics. The plume—which essentially measures the climatological intensity of the “tape recorder” effect (Mote et al. 1996, 1998)—is seen to wobble a bit northward and then southward on its vertical “ascent.” Above 10 hPa this feature merges into the upper stratospheric pattern. The residual variance of water vapor (Fig. 1d) is similar to that of methane but includes a shallow layer of enhanced variance above the tropopause and a second shallow layer or “arm” of variance extending across the equator between 22 and 10 hPa. Generally there is more residual variance in water vapor than can be accounted for by methane oxidation.

Ozone presents a different picture in nearly every respect. This photochemically active constituent has maximum concentration in the tropical middle stratosphere and a broad region of low concentration in the tropical lowermost stratosphere. The climatological variance (Fig. 1e) is confined mainly to the subtropics and extratropics, in three distinct layers. The residual variance, on the other hand, appears mainly in the Tropics (Fig. 1f). Two lobes are centered on the equator and another pair straddle the equator, the northern lobe being about 50% stronger.

#### *b. Interannual variability*

For residual or “seasonally adjusted” variations of tracer, nine EOFs were rotated, of which the first four explain approximately three-fourths of the variance. In methane, 73.2% of the residual variance is explained by the first four EOFs, and each has a fairly simple structure (Fig. 2) and time dependence (Fig. 3). Our display of principal component time series in Fig. 3 is augmented by a bandpass filtered series (dotted line) and sinusoidal curve fit (thick solid line) assuming a simple harmonic dependence, the details of which are discussed in the next section. In Fig. 2, the first EOF is approximately symmetric about the equator and occupies the region of large residual variance in the equatorial upper stratosphere. The time series is quasi-biennial, with clear evidence of advancing phase through the calendar year, except for the last QBO cycle, which had a period of 24 months, as discussed in section 5. This EOF is similar

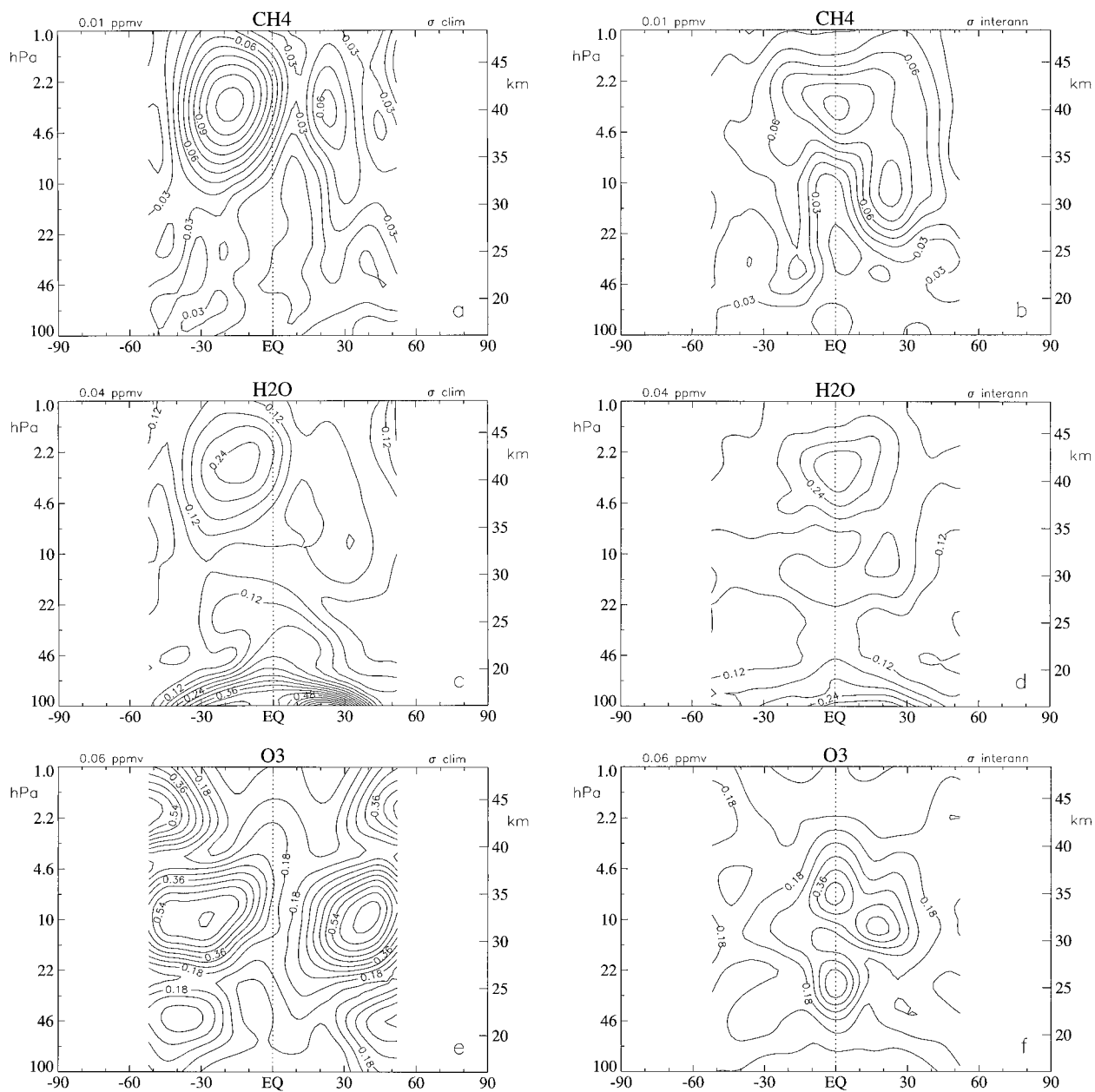


FIG. 1. Variance statistics derived from HALOE data for 1992–99. (a), (b) Methane; (c), (d) water vapor; (e), (f) ozone. The standard deviation of climatological variation is shown in (a), (c), (e); the standard deviation of residual variation is shown in (b), (d), (f). Units: ppmv.

to the leading mode of SVD between HALOE methane and monthly mean Singapore rawinsonde data shown in Fig. 22 of Randel et al. (1998). The second and third EOFs are antisymmetric, each having a quadrupole pattern. A tilted quadrupole was found by Randel et al. in their second SVD mode. Here there are two quadrupole EOFs, neither of which tilt much. Of the two EOFs, the first antisymmetric EOF better approximates the second SVD mode of Randel et al. (1998): both have largest amplitude in the northern subtropics near 10 hPa. The time series of antisymmetric EOFs could be described

as “subbiennial” with period slightly less than 2 yr, except for the last cycle in which the period stretches to about 24 months. If the subbiennial variation is attributable to QBO–annual cycle interaction, an *increase* of subbiennial period toward 24 months should accompany a *decrease* of QBO period toward 24 months; the time series in the last 2 yr are consistent in this respect. The second antisymmetric EOF leads the first, implying a peculiar *upward* propagation of the methane anomaly in the subtropics. The fourth EOF somewhat resembles an SAO EOF from the methane climatology, with anom-

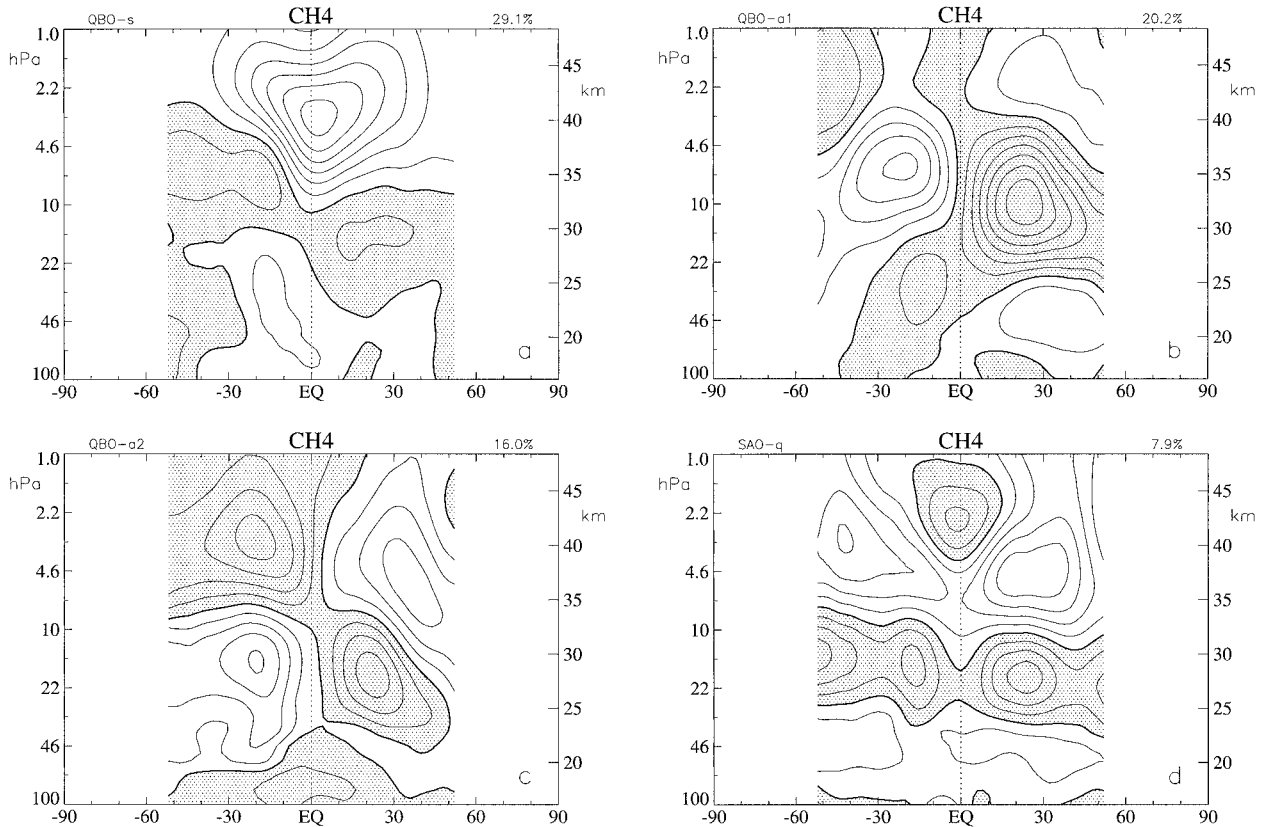


FIG. 2. Rotated EOFs of seasonally adjusted methane, normalized to unit variance. Shading indicates negative values.

ally maxima at equinox in the westerly phase of the stratopause SAO. Unlike the climatology, these positive anomaly maxima occur only in a particular phase of the QBO. Their effect is to enhance the SAO double peak below the stratopause in the “deep westerly” phase of the QBO as documented previously by Ruth et al. (1997), Kennaugh et al. (1997), and Randel et al. (1998). The sinusoidal curve fit (with QBO period) is less accurate in this case, compared to that of the other three EOFs.

The four leading EOFs of seasonally adjusted water vapor, shown in Fig. 4, explain 69.6% of the residual variance. For this calculation the lowest three stratospheric levels were excluded in order to de-emphasize tape recorder variations near the tropopause that would otherwise appear as two EOFs located between two sets of QBO related EOFs. The first EOF corresponds to that of methane in the upper stratosphere, with time series exactly out of phase and once again displaying QBO phase progression through the calendar year, except for the last cycle, as shown in Fig. 5. The second and third EOFs are subbiennial, their time series positively correlated with the third and second EOFs of methane, respectively, but with EOFs of opposite sign, each containing elements of the quadrupole patterns of methane EOFs. Thus, the corresponding anomalies in physical space are negatively correlated, as in the first EOF. The

third and fourth EOFs of water vapor explain the arm of residual variance extending across the equator between 10 and 22 hPa (Fig. 1d). It may be that variations of tape recorder ascent due to the QBO are responsible for this arm that is unique to water vapor and does not appear in methane. Water vapor, moreover, contains subbiennial variability at the equator. As with methane, the sinusoidal curve fit of the fourth EOF is imperfect, especially in the first cycle. The contribution from the fourth EOF is small, however, in both tracers.

The leading EOFs of seasonally adjusted ozone, shown in Fig. 6, explain 68.9% of the residual variance. The first EOF is somewhat antisymmetric near 10 hPa and explains the variance maximum near 20°N. The fourth EOF, although noisy, is rather like a mirror image of the first, explaining the smaller variance maximum near 16°S. The time dependence of the first EOF is subbiennial (Fig. 7), but the fourth EOF contains a mixture of frequencies and is only partly explained by its subbiennial harmonic. The second and third EOFs represent quasi-biennial fluctuations with the second leading the third, implying downward phase propagation at the equator. Their structure is similar to the SVD modes of Randel and Wu (1996). Unlike the dynamical QBO (Dunkerton 2000), the ozone QBO has several extrema stacked on the equator, giving the (misleading) appearance of slower phase descent. This is attributable to the

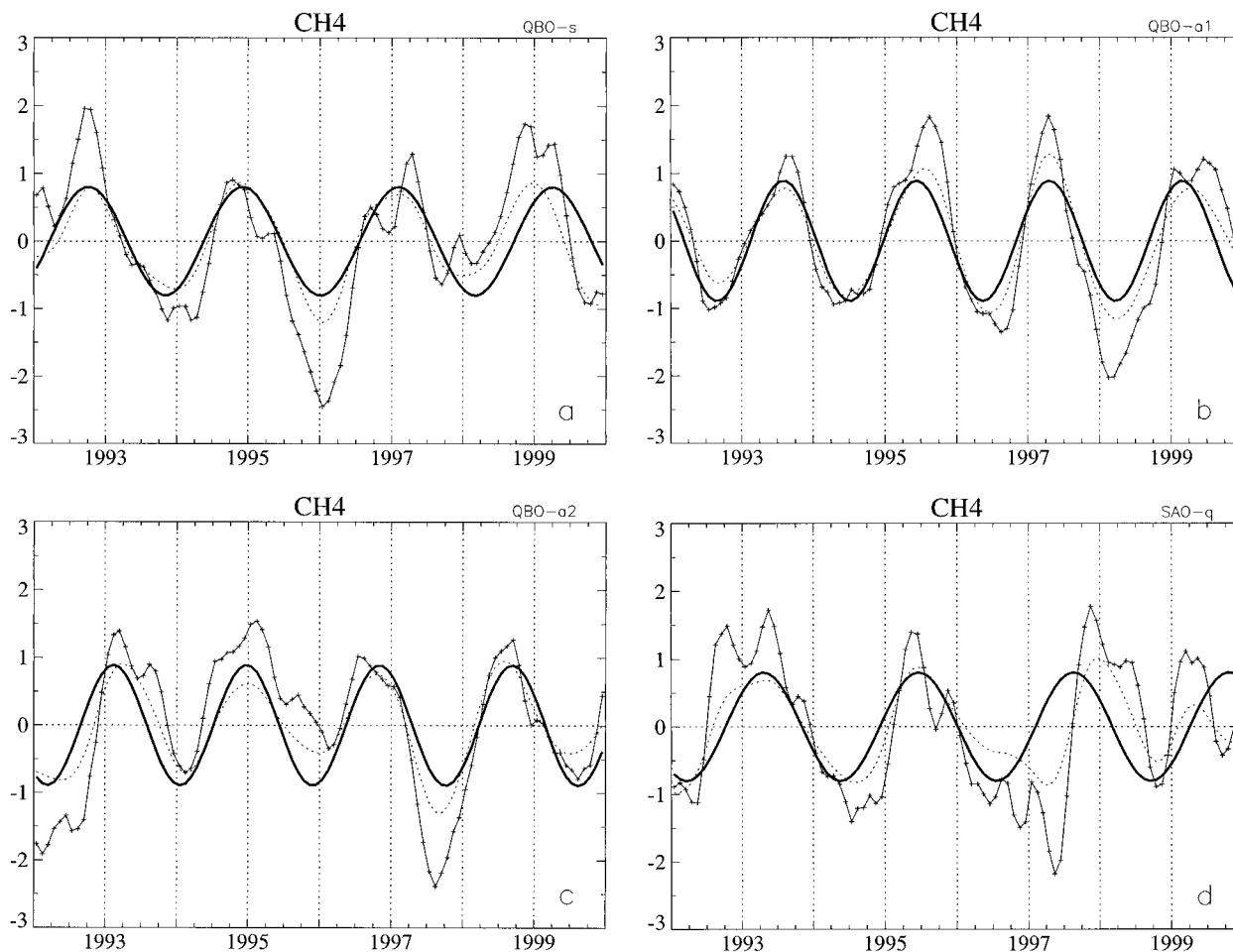


FIG. 3. Principal components of methane corresponding to the rotated EOFs of Fig. 2. Symbols indicate original time series; dotted curves display bandpass filtered data; heavy solid curves indicate a quasi-biennial or subbiennial harmonic, obtained by a least squares fit, subject to certain constraints (see text).

combination of photochemical and dynamical control at upper and lower levels, respectively. Ozone anomalies near 30 km are thought to arise from  $\text{NO}_y$  anomalies (Chipperfield et al. 1994; Politowicz and Hitchman 1997), but in the upper stratosphere the temperature anomaly may be more important (Jones et al. 1998). Temperature fluctuations necessarily have zero latitudinal gradient at the equator, if in balance with the mean zonal wind; this explains the symmetric pattern of ozone variation in the upper stratosphere (in semiannual and interannual EOFs). Methane and water vapor EOFs (including those of “symmetric” type) do not exhibit such precise symmetry at this altitude.

In summary, the three leading EOFs of seasonally adjusted water vapor match those of methane reasonably well, and the time series suggest that the anomalies are anticorrelated in physical space, as expected if due to transport acting on tracer gradients of opposite sign. The two sets of EOFs were obtained independently. Ozone has a unique structure, but like the other two constituents, contains subbiennial as well as quasi-biennial var-

iations. Quasi-biennial variations are found near the equator while most, but not all, of the subbiennial variation occurs in the subtropics. Water vapor, and to a lesser extent ozone, display subbiennial variability at the equator, together with quasi-biennial variation.

#### 4. Reconstruction of trace constituent fields

##### a. Overview

Time–latitude plots of seasonally adjusted methane in the upper and middle stratosphere are shown in Fig. 8, reconstructed from the first four rotated EOFs. The percent variance explained *on each grid level* is indicated on the title row. A truncated set of EOFs may be used as a filter to highlight the most important variations in the data. In the upper stratosphere, methane anomalies propagate from the equator to the northern subtropics (Fig. 8a). This relationship falls apart toward the end of the record. In the latter half, propagation develops from the equator to the southern subtropics. In the mid-

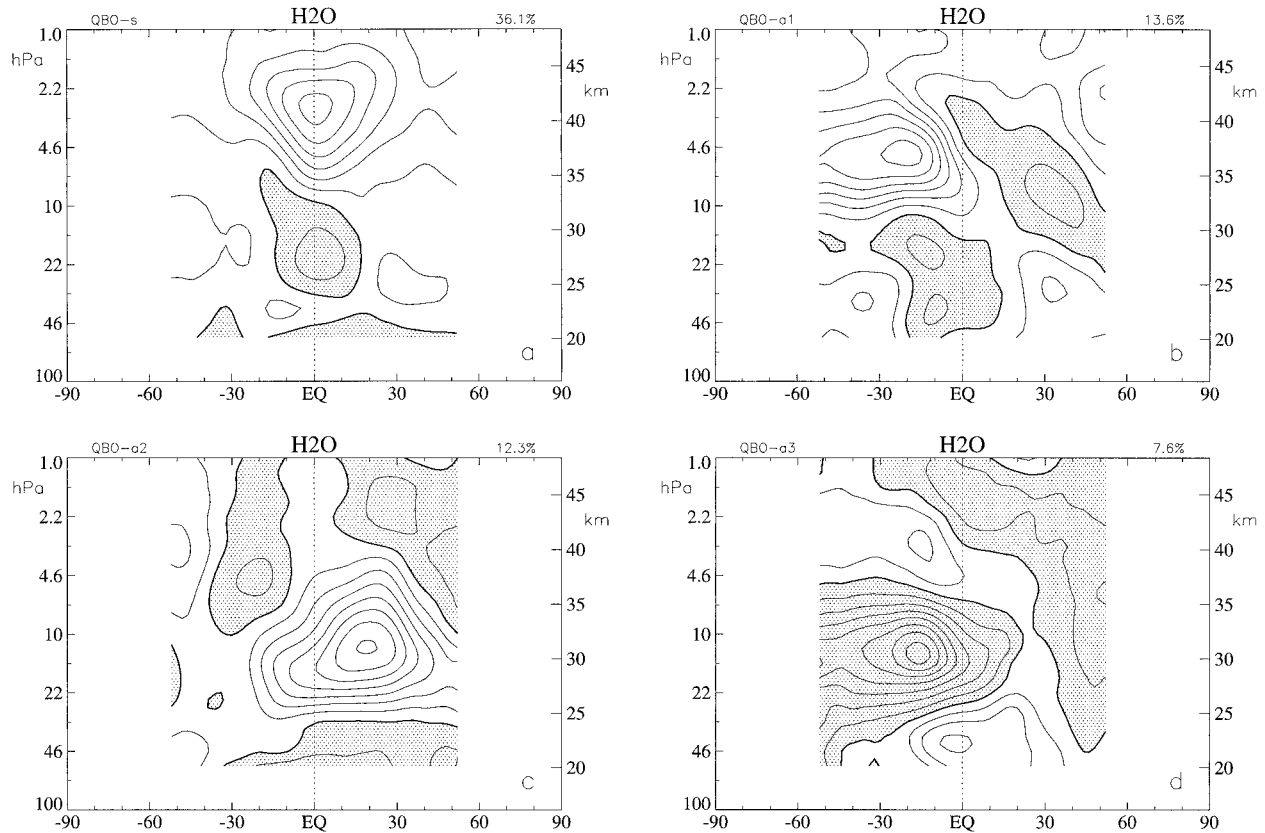


FIG. 4. Rotated EOFs of seasonally adjusted water vapor, normalized to unit variance. Shading indicates negative values.

dle stratosphere, anomalies are observed mainly in the northern subtropics and are rather well synchronized with the seasonal cycle, most centered within 3 months of northern spring equinox (Fig. 8b). These results may be compared to Figs. 25 and 26 of Randel et al. (1998) showing the entire anomaly field at nearby levels.

The corresponding plots of seasonally adjusted water vapor (not shown) display anomalies opposite in sign to those of methane with similar features and additional variation near the equator in the middle stratosphere. Figure 27 of Randel et al. (1998) shows the entire anomaly field at 10 hPa.

The seasonally adjusted ozone (not shown) was examined on the three levels containing maxima of residual variance. At 6.8 hPa, equatorial anomalies are flanked by anomalies in the northern subtropics. Later, toward the end of the record, anomalies appear in the southern subtropics. Comparison to Fig. 28 of Randel et al. (1998) suggests that these ozone anomalies are well correlated with anomalies of residual vertical velocity at 10 hPa. This would be expected if (i) 6.8- and 10-hPa vertical velocities are similar, apart from a small phase lag due to QBO phase descent; (ii) vertical velocity and temperature anomalies are anticorrelated (due to radiative damping); and (iii) temperature and ozone anomalies are anticorrelated (due to a self-healing effect). There is some similarity between 6.8 and 10 hPa,

but ozone anomalies at 10 hPa are larger off the equator, while anomalies at 26 hPa are centered on the equator.

#### b. Least squares fit

In general, equatorial anomalies display quasi-biennial variation with evidence of advancing phase through the calendar year. Thus, if subtropical anomalies are synchronized with the seasonal cycle, or have subbiennial period, the relationship between equatorial and subtropical anomalies must change slowly with time. The tendency in Fig. 8a for anomalies to link at first with the northern subtropics and then with the southern subtropics indicates such a changing phase relationship, as in column ozone (Hasebe 1984; Lait et al. 1989; Gray and Dunkerton 1990). This change is illustrated more clearly in Fig. 9, showing a reconstruction of the methane anomaly in which the original principal component time series were replaced by their quasi-biennial or subbiennial harmonics obtained with a least squares fit. To digress briefly, the heavy solid curves in Figs. 3, 5, and 7 were obtained by a least squares simultaneous fit of quasi-biennial and subbiennial harmonics to the principal components of symmetric and antisymmetric EOFs, respectively, requiring that the time series within each pair of quasi-biennial and subbiennial harmonics be in quadrature. The period of subbiennial variation

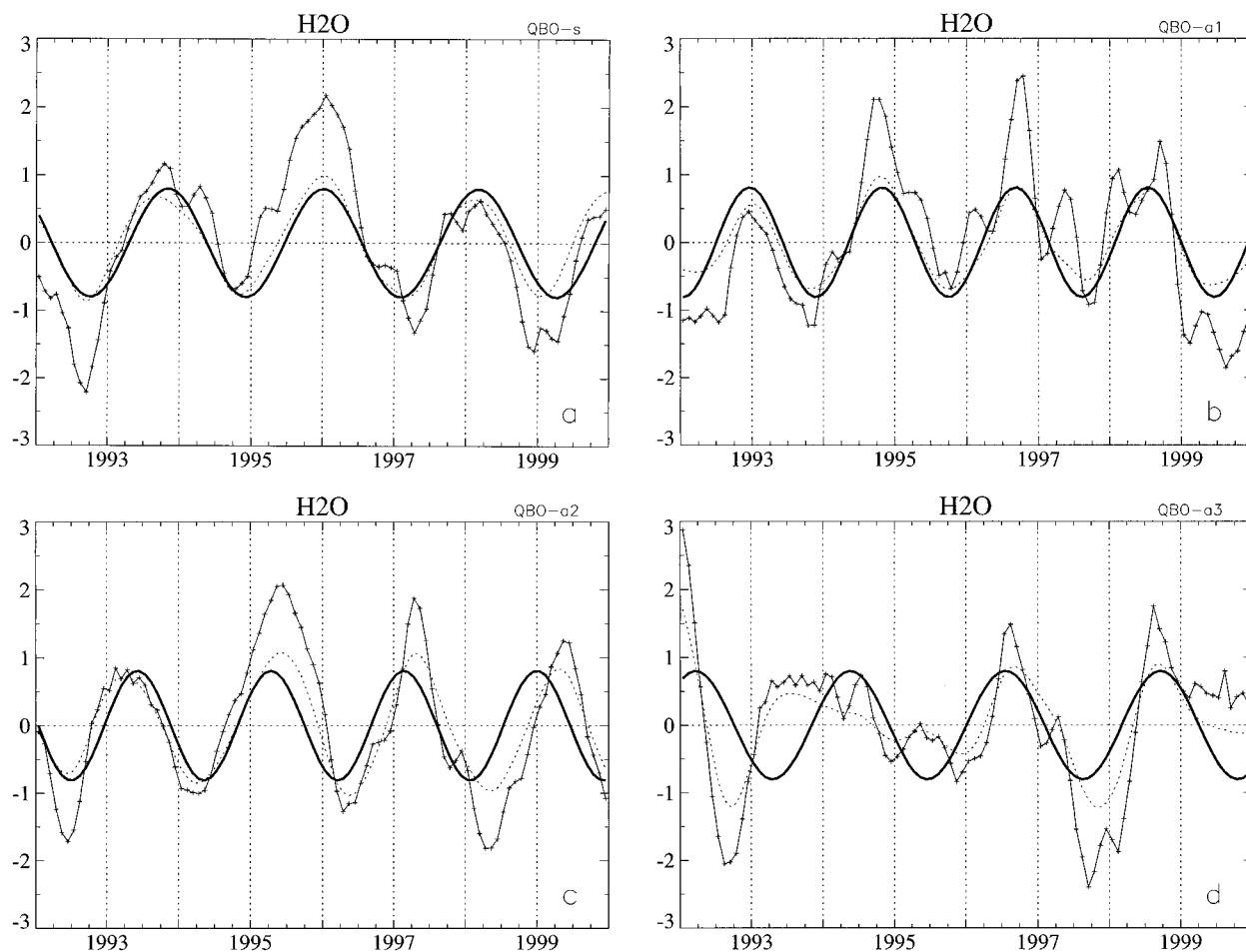


FIG. 5. As in Fig. 3, but for principal components of water vapor corresponding to the rotated EOFs of Fig. 4.

was constrained by Eq. (5.2) below. For each curve fit, the amplitude was determined by the variance of the corresponding bandpass filtered series. Only three parameters were varied to obtain the least squares fit: the QBO period, QBO phase, and subbiennial phase. This calculation was performed on the three tracers independently, but the same QBO period was obtained in each case, namely, 26 months. The corresponding subbiennial period is 22.3 months, and in this case, 13 yr are required for the QBO to advance completely through a calendar year. Thus, in the 8-yr HALOE data record the decadal cycle of QBO modulation is incomplete, a problem further aggravated by a contraction of QBO period to 24 months in the last cycle.

By substituting curve fits for the original principal components, the latter problem is alleviated, without much loss of accuracy. The final anomalies in Figs. 8 and 9 match well, despite a slight lengthening of QBO phase in the fitted data. Figure 9 provides an idealization of the anomaly behavior in Fig. 8, clearly showing a slow decadal modulation of tropical–subtropical relationship. Since only 8 yr are shown, the modulation cycle is incomplete. Figure 10 extends the series, dis-

playing the squared anomalies obtained from fitted data. The changing pattern undergoes a complete cycle in 13 yr. The data after 1999 are bogus, of course, and we cannot assume that the QBO period is a constant 26 months, this assumption having already been violated in the 1998/99 cycle. The value of Fig. 10 will become clear at the end of this section when discussing the climatology of anomaly variance.

A further caution regarding the extrapolation in Fig. 10 is that the underlying EOF structures (Figs. 2, 4, 6) are assumed not to change with time as new data are added. Comparison of a shorter (6-yr, HALOE version 18) dataset with the present (8-yr, HALOE version 19) dataset indicated no significant change in the leading three EOFs, while the temporal dependence of the fourth EOF became slightly easier to interpret with additional data. Therefore it is unlikely that any qualitative changes will be observed when data after 1999 become available. Note, however, that not all combinations of QBO and annual cycle have not been realized in this time interval (section 5), so it remains possible that the EOFs may change in a minor quantitative way; for example, they may become more symmetric or antisymmetric about

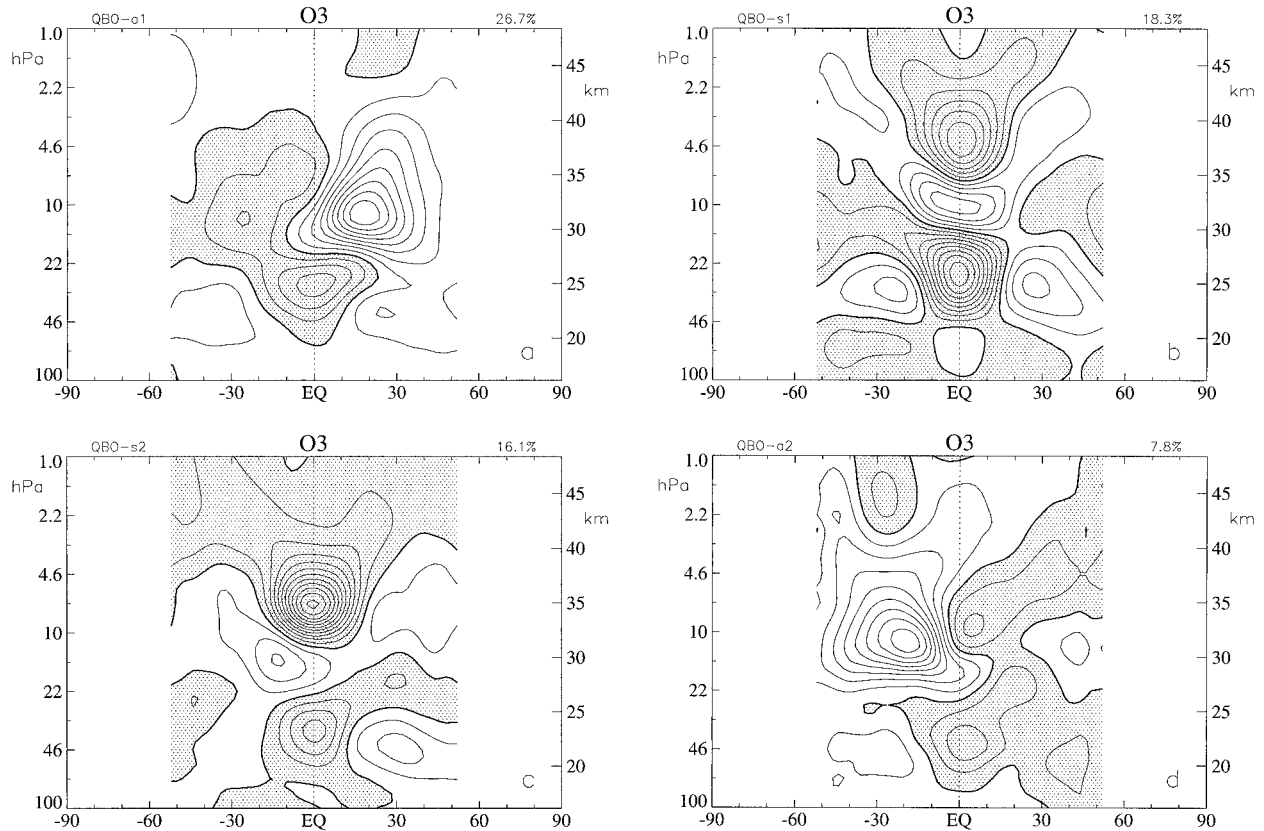


FIG. 6. Rotated EOFs of seasonally adjusted ozone, normalized to unit variance. Shading indicates negative values.

the equator. In what is probably a worst-case scenario, the addition of new data may indicate stronger anomalies in the Southern Hemisphere middle stratosphere, yielding a less lopsided distribution of variance among antisymmetric EOFs than is presently observed.

In Figs. 3, 5, and 7 the curve fit for the fourth mode's time series is substantially worse than that of the first three; therefore, the reconstruction of variance was repeated without the fourth EOF. Similar results were obtained concerning the location and seasonal timing of anomaly maxima, as the fourth mode's contribution is relatively small.

### c. Vertical structure

We note incidentally that there is a changing phase relationship between tracer anomalies in the middle and uppermost stratosphere, especially noticeable in the subtropics. The equatorial methane anomaly (not shown) is like that in Fig. 19 of Randel et al. (1998). At 24°N the methane anomaly propagates upward, but the rate of "propagation" diminishes with time, consistent with the observation that anomalies in the middle stratosphere are more closely synchronized with the seasonal cycle (maximizing in Northern Hemisphere spring, north of the equator) while QBO variation is dominant in the upper stratosphere, throughout the Tropics and

subtropics. The story is similar for water vapor, with the added complication that the equatorial anomaly is significant below 10 hPa and near the tropopause. The subtropical variation shows clearly that the upward propagation is slowing down. The upper stratospheric signal in methane and water vapor originates primarily in their leading EOF, which extends into the subtropics (Figs. 2a, 4a) and has a true quasi-biennial variation (Figs. 3a, 5a).

In time–height cross sections of seasonally adjusted ozone (not shown) the equatorial QBO is seasonally asynchronous and displays a slow downward propagation, presumably due to the transition from photochemical to dynamic control as QBO phases descend. The rate of descent in each region is comparable to that of the dynamical QBO, separated by a node near 10 hPa (Zawodny and McCormick 1991). The subtropical signal is seasonally synchronized and confined to the middle stratosphere.

### d. Anomaly variance climatology

Noting a tendency for anomalies to appear preferentially at certain times of the year, in certain places, it is useful to quantify their apparent seasonal synchronization. Synchronization of subtropical column ozone was found by Hamilton (1989) and others. Evidently

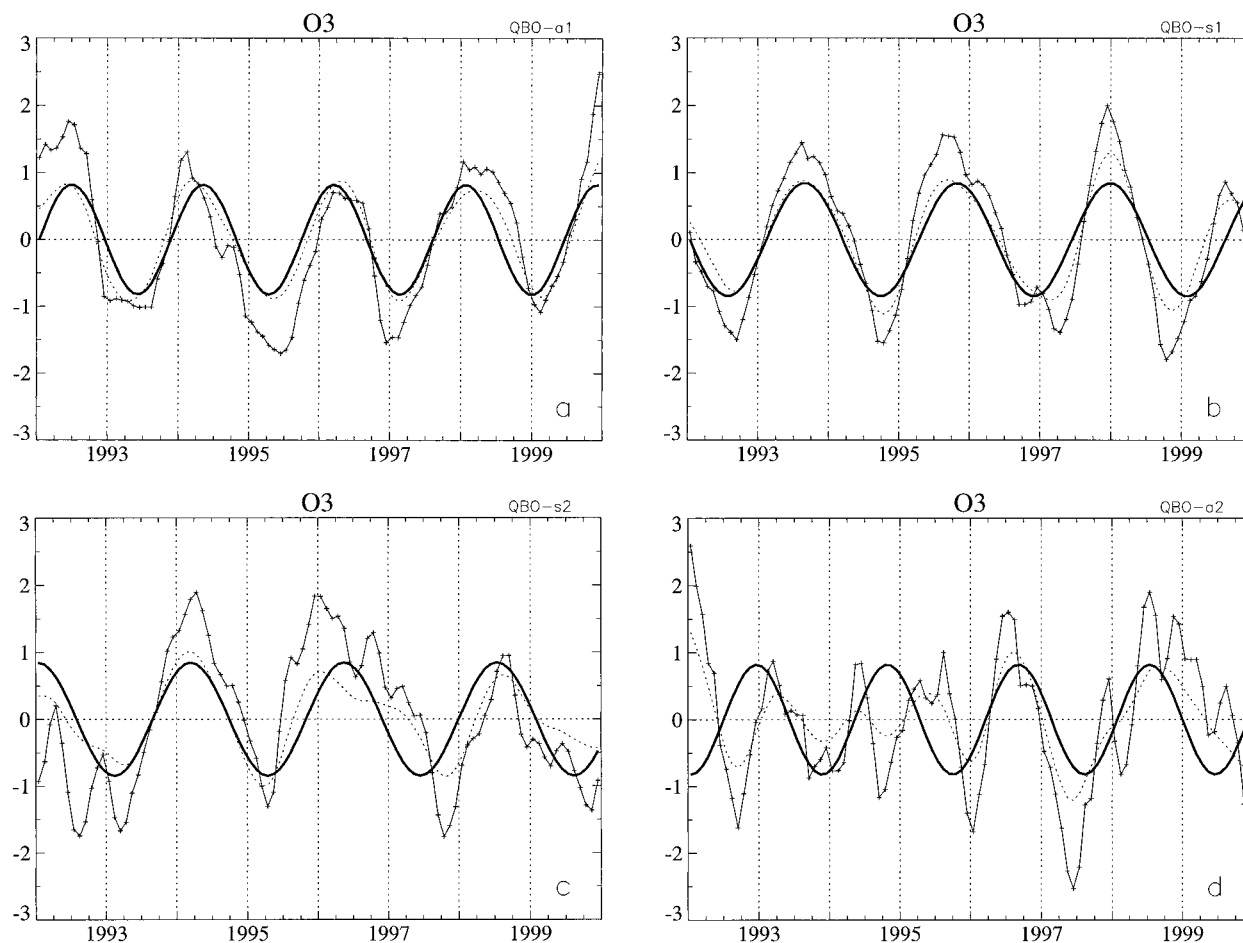


FIG. 7. As in Fig. 3, but for principal components of ozone corresponding to the rotated EOFs of Fig. 6.

some, but not all, of the HALOE mixing ratio variations within the stratosphere are modulated or synchronized by the seasonal cycle. While the original data display a somewhat bewildering pattern (Fig. 8), the fitted data provide a clearer picture (Fig. 9), allowing a second estimate of synchronization in addition to that of the original data. In Fig. 11 the climatology of anomaly variance is shown, for methane at two levels, and for water vapor at one level. Figures 11a–c were derived from the original 8 yr of reconstructed data, using the leading four EOFs. Figures 11d–f were obtained from the harmonic fit, extrapolated over a 13-yr modulation cycle, an example of which was shown previously in Fig. 10. Both methods have limitations: in the first method, the modulation cycle is incomplete; in the second method, the harmonic fit is imperfect. Similar results were obtained, nonetheless, with minor differences that will be noted below.

For methane in the upper stratosphere (Figs. 11a,d) there is a branch of large variance extending into the northern subtropics, maximizing in late northern winter, while a second branch propagates from 5°S to the southern subtropics, maximizing at southern spring equinox.

In Fig. 11d, these branches are separated by a well-defined minimum in the *annual range of anomaly variance* near 5°N. It is noteworthy that the minimum of annual range occurs near the point of maximum anomaly variance in the upper stratosphere. The equatorial variance of methane is almost asynchronous, as it must be if dominated by the first EOF, and its temporal variation is replaced with that of a 26-month QBO harmonic that is perfectly asynchronous. In the middle stratosphere (Figs. 11b,e) the methane anomaly north of the equator prefers northern spring equinox; a much weaker anomaly also appears in the Southern Hemisphere near southern spring equinox. There is a hint of semiannual variation south of the equator. These results are consistent with Fig. 8, and are representative of methane variations throughout the middle and upper stratosphere.

For water vapor, the seasonal variation in the subtropical upper stratosphere is rather similar to that of methane (not shown), but a different picture is obtained in the middle stratosphere (Figs. 11c,f). In Fig. 11c, the anomaly south of the equator is relatively larger than that of methane, and somewhat earlier. In Fig. 11f, this difference is exaggerated: the pattern of climatological

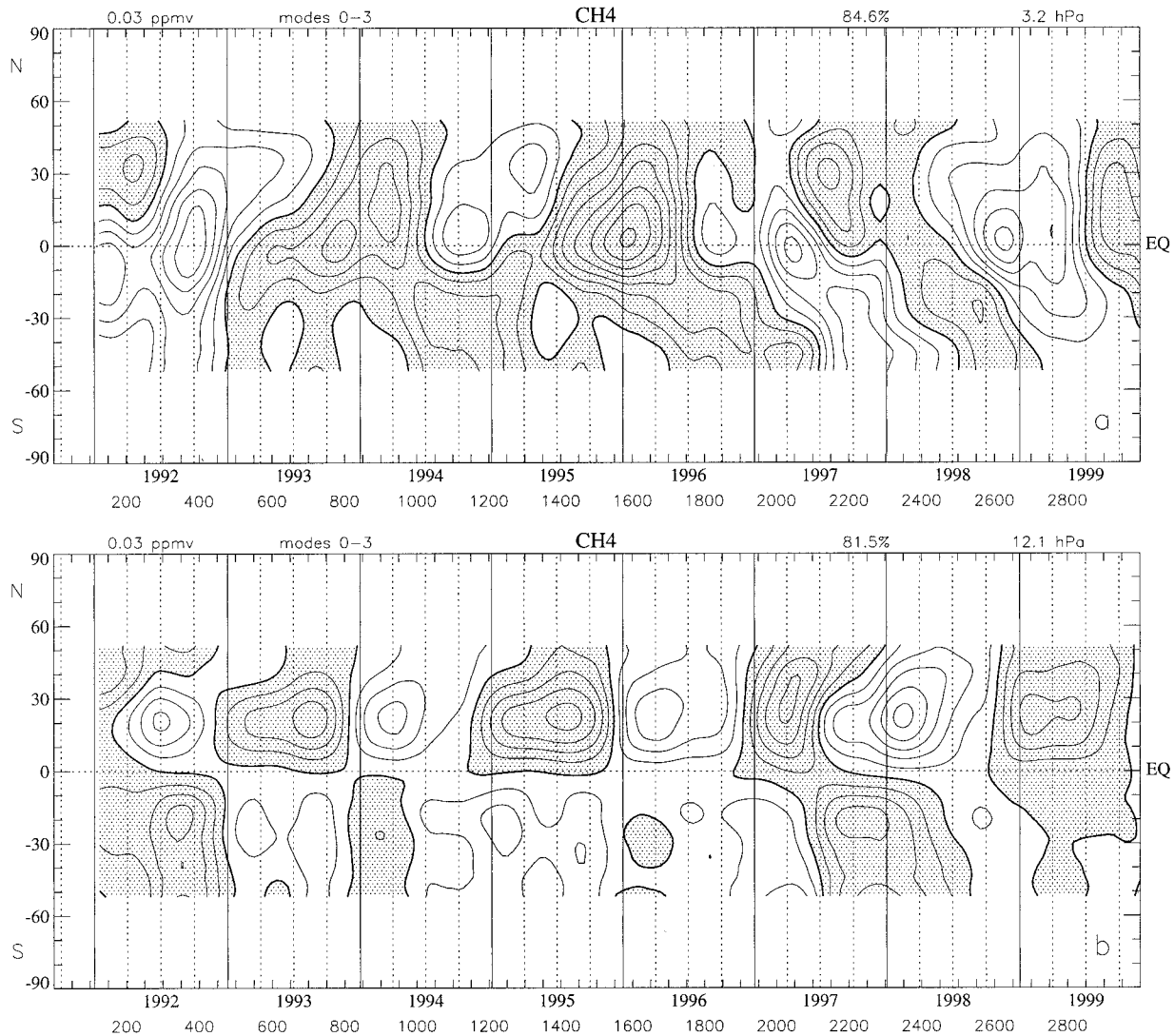


FIG. 8. Time-latitude cross sections of methane anomalies reconstructed using the first four rotated EOFs of seasonally adjusted data. Shading indicates negative values. Contour interval: 0.03 ppmv, (a) 3.2 hPa, (b) 12.1 hPa.

anomaly variance straddles the equator, centered in Northern Hemisphere spring. Comparison with original data, showing the actual times of off-equatorial anomaly extrema, suggests that Fig. 11c is more accurate than Fig. 11f, south of the equator (based on 8 yr of data). The discrepancy between the two figures can be attributed, in part, to the first cycle of the fourth principal component time series (Fig. 5d), which is not well described by the harmonic fit.

Because the modulation cycle is incomplete in HAL-OE data currently available, we cannot be certain which picture (Fig. 11c or 11f) is correct south of the equator. The two patterns of anomaly variance do, however, agree at and north of the equator. Thus, the behavior of water vapor in the middle stratosphere differs sharply from that of methane in two ways. First, the equatorial water vapor anomaly is significant, whereas a methane

anomaly is virtually absent at this level. Second, the phase of water vapor anomaly is more symmetric about the equator, contrary to that of methane in which subtropical anomalies appear 6 months apart.

This observation implies that (i) a different mechanism is responsible for the equatorial water vapor anomaly in the middle stratosphere, and (ii) the equatorial anomaly alters the timing of the off-equatorial anomaly, shifting the Southern Hemisphere anomaly to an earlier time by 1–4 months relative to that of methane. It was suggested that QBO related variations of tape recorder ascent may contribute to the equatorial anomaly. Ascending water vapor anomalies in the equatorial time-height cross section, to be reported elsewhere, support this view. We note that variations of vertical transport, approximately symmetric about the equator, would create anomalies with symmetric phase, unlike the merid-

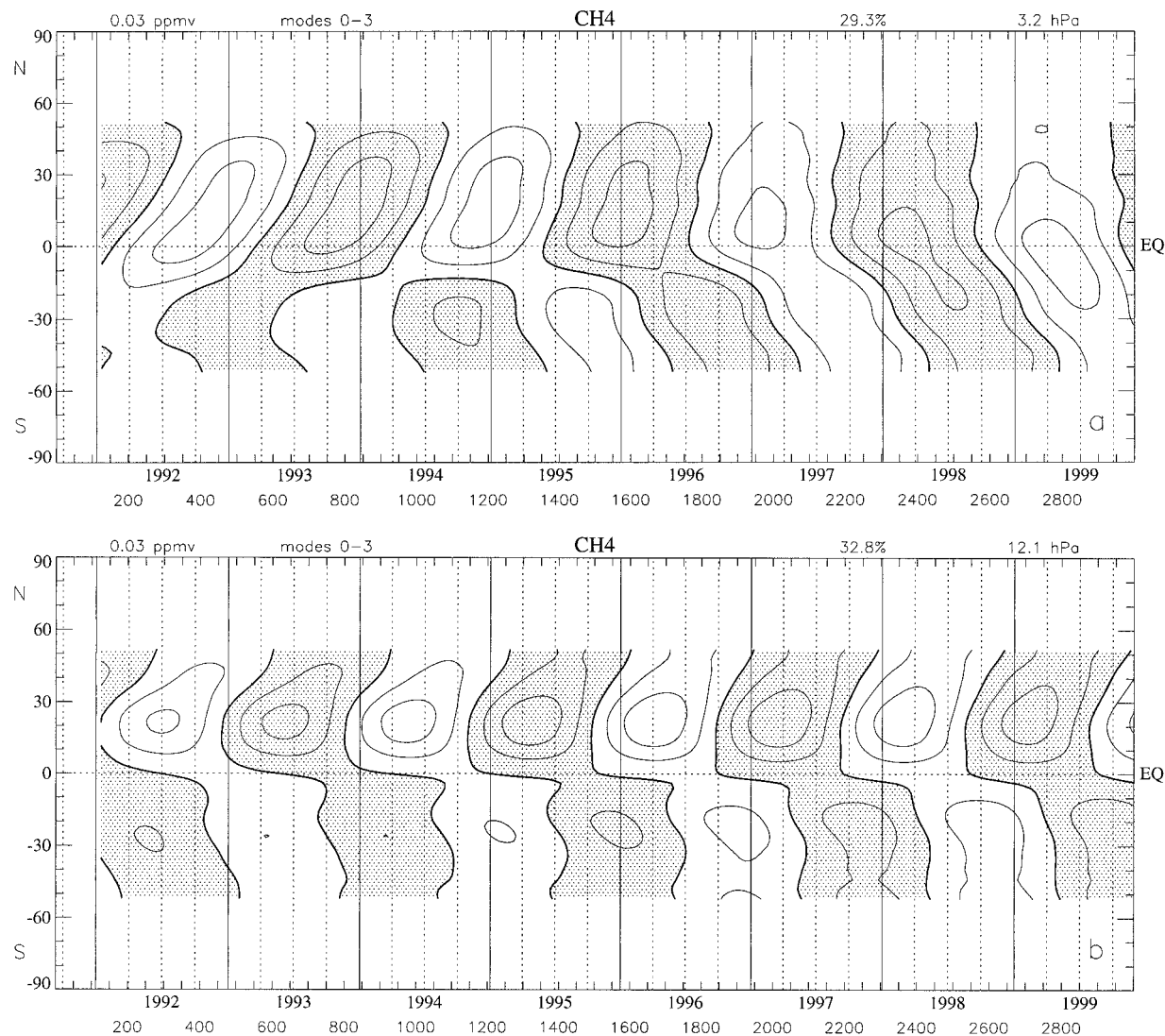


FIG. 9. Time–latitude cross sections of methane anomalies reconstructed as in Fig. 8, but with quasi-biennial and subbiennial harmonics from a least squares fit substituted for the original principal component time series.

ional transport, which, if also approximately symmetric about the equator, would produce anomalies with antisymmetric phase.

For ozone, seasonal synchronization is observed north of the equator, mainly near 10 hPa, and in a small patch below 22 hPa, centered on the equator (not shown). The latter feature displays rapid phase variation with height and may be spurious, attributable to sampling errors associated with the QBO. The absence of seasonal synchronization in the equatorial middle and upper stratosphere is consistent with the photochemical or dynamical control of ozone anomalies by the QBO, driven by local QBO anomalies of temperature,  $\text{NO}_y$ , or vertical velocity. These equatorial anomalies are less sensitive (than those of methane or water vapor) to meridional transport variations associated with the annually varying Brewer–Dobson circulation. Our results, based

on mixing ratio rather than on number density, tend to emphasize ozone anomalies in the middle and upper stratosphere and should not be thought to contradict the results of Hamilton (1989) and others, derived from column ozone. Similar EOF analysis based on number density, rather than on mixing ratio, would expose the seasonal variation of lower stratospheric ozone anomalies more clearly.

## 5. Relation to the dynamical QBO

### a. Temporal relationship

As shown by Wallace et al. (1993) the near-equatorial QBO can be represented by the two leading principal components of Singapore rawinsonde data. Their trajectory (in the phase space spanned by these two EOFs)

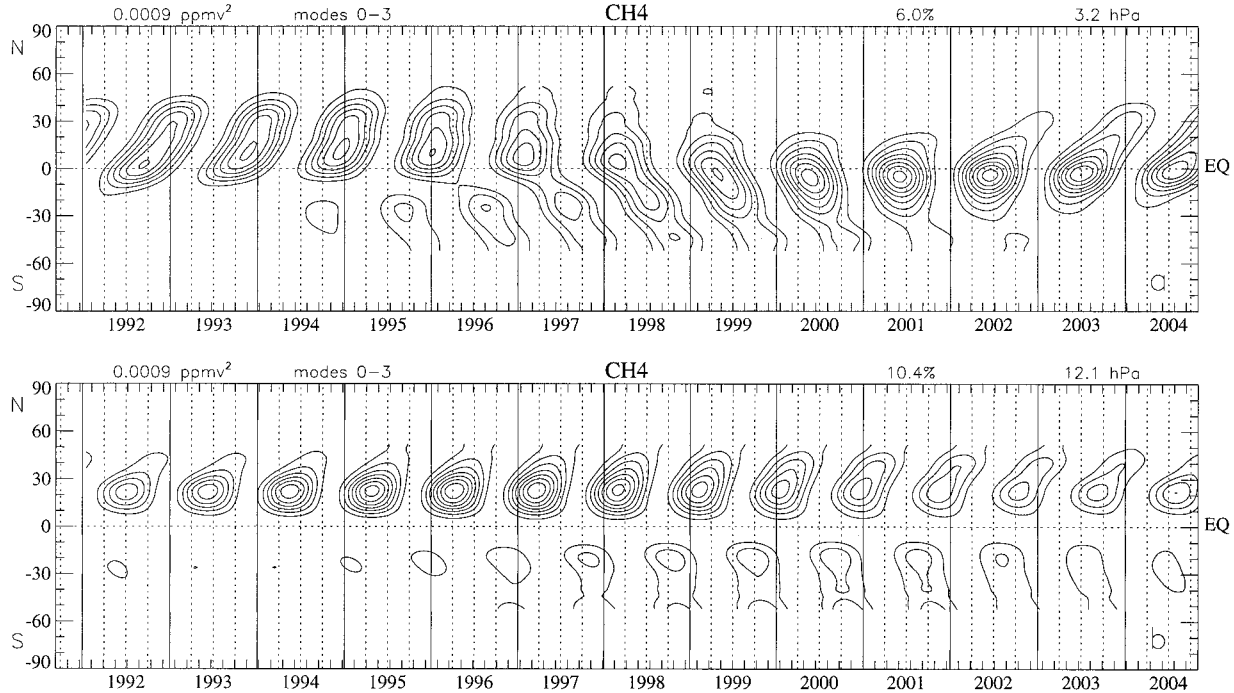


FIG. 10. Time-latitude cross sections of squared methane anomalies derived from Fig. 9, extrapolated to a full modulation cycle of 13 yr.

is nearly circular and may be used to define a QBO phase *angle*—an improvement over the traditional binary definition of QBO phase as “easterly” or “westerly” at some level. The time series of QBO modes derived from UKMO analyses (Dunkerton 2000) likewise may be used for this purpose, as shown in Fig. 12. Plotted against one another, these series trace a counterclockwise revolution that is reasonably circular, but with a variable rate of phase progression. For example, note the slow onset of QBO easterlies in the lower right quadrant, just below the positive  $x$  axis. Slowing of easterly shear-zone descent is common between 30 and 50 hPa (Naujokat 1986). The thick curve provides a fit to the QBO amplitude, while allowing the period of the QBO to vary with time. Although in reality QBO amplitude is not exactly constant, the QBO departs from a perfect sinusoid mainly in its rate of phase progression and possible synchronization with the seasonal cycle (Dunkerton 1990; Wallace et al. 1993; Dunkerton and Delisi 1997).

The phase of the QBO may be defined, without reference to a particular level, as

$$\tan\phi_{\text{QBO}} = \frac{R(\text{QBO}_d)}{R(\text{QBO}_m)}, \quad (5.1)$$

where  $R$  signifies the rotated principal component time series; “d” and “m” refer to the QBO dipole and monopole EOFs defined in Dunkerton’s (2000) analysis of UKMO data. One may then visualize the phase of the dynamical QBO relative to the annual cycle in a phase diagram as shown in Fig. 13. Here the phase of the

annual cycle was defined simply as a phase angle varying from zero on 1 January to  $2\pi$  on 31 December. An alternative definition, using the two principal components of the annual cycle, gave similar results. Dotted lines show the trajectory of the QBO relative to the annual cycle, one dot per pentad corresponding to the time resolution of low-pass filtered UKMO data. Circles indicate approximately the middle of each month corresponding to the resolution of monthly mean HALOE data. Time increases upward and to the right. Each trajectory passes a little below the preceding one because the QBO period is slightly longer than 2 yr, except for the last QBO cycle, indicated by solid circles, having a period of about 24 months. Note that the solid circles return to their starting point at the completion of the last cycle. Only a fraction of the diagram is occupied by data points during the UKMO record from 1991 through 1998, indicating a small advance of QBO phase through the calendar year, as suggested by the time series themselves. As a result, all possible combinations of QBO and annual cycle phase have not been realized in this time interval.<sup>1</sup> This has important implications for QBO related anomalies in stratospheric trace con-

<sup>1</sup> If the QBO were exactly synchronized with the seasonal cycle, the phase diagram would never fill up but rather would contain an integral number of discrete pathways. A longer record shows that while the phase diagram is tending to fill up as the decades go by, certain areas have a denser concentration of trajectories than others (Dunkerton 1990; Wallace et al. 1993).

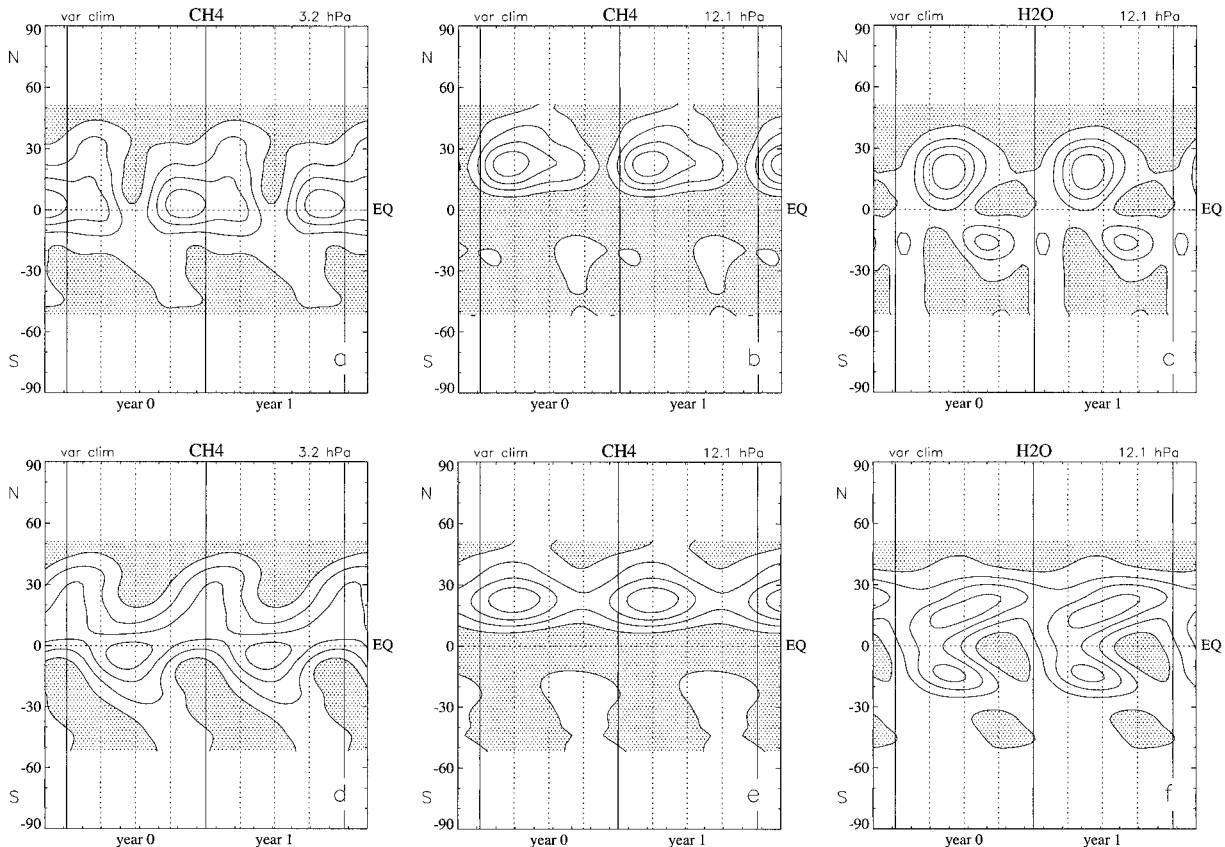


FIG. 11. (a), (b) Variance climatology of methane anomalies derived from reconstructed data based on the original principal component time series extending over 8 yr, 1992–99. (c) As in (b), but for water vapor. (d), (e) Variance climatology of methane anomalies derived from reconstructed data based on a harmonic fit to the principal component time series, extrapolated to a full 13-yr modulation cycle as in Fig. 10. (f) As in (e), but for water vapor. Data were normalized by the maximum value in each panel; contour interval is 0.2, with smaller values shaded.

stituents observed during the *UARS* period. Subtropical QBO anomalies, in particular, have thus far been observed mainly in the Northern Hemisphere.

Evident in the figure is a clustering of 46-hPa easterly onsets in northern spring (Dunkerton 1990) preceded by a slowdown in the rate of phase progression, that is, slowing of easterly shear-zone descent near 46 hPa. Although the dynamical QBO is asynchronous, easterly onsets near 46 hPa cluster in northern spring after a temporary “stall” in northern winter during which the QBO phase does not advance. This behavior was noted by Dunkerton (1990) and has continued through the *UARS* observing period.

The variation of HALOE trace constituents in relation to the dynamical QBO and annual cycle is shown in Figs. 14a–i for the three leading principal components of seasonally adjusted methane, water vapor, and ozone. The symbol area is proportional to principal component value; open (filled) circles denote positive (negative) values. Equatorially symmetric EOFs (suffix “s”) are asynchronous and depend only on the phase of the QBO, indicated by a horizontal symbol pattern. “Antisymmetric” EOFs (suffix “a”) display a more complicated

pattern. If these modes are subbiennial, with frequency  $\omega_s$  determined by the difference interaction of annual and QBO harmonics,

$$\omega_s = \omega_A - \omega_Q, \quad (5.2)$$

then the slope of the symbol pattern should be +1 on the phase diagram. This is shown trivially by the definition of phase as frequency multiplied by time, plus a constant, assuming that the frequency itself is constant in time. Any function of subbiennial phase is also a function of the difference between annual and QBO phases. By the same reasoning, the slope is  $-1$  for the sum interaction  $\omega_A + \omega_Q$ .

#### b. Spatial relationship

The leading EOF of HALOE methane has positive sign in the equatorial upper stratosphere (by definition), and its principal component attains largest negative value around a QBO phase of  $-\pi/4$ , corresponding to the westerly onset near 2.2 hPa (Fig. 12). This agrees with the observation of Randel et al. (1998) that methane anomalies in the upper stratosphere are positively cor-

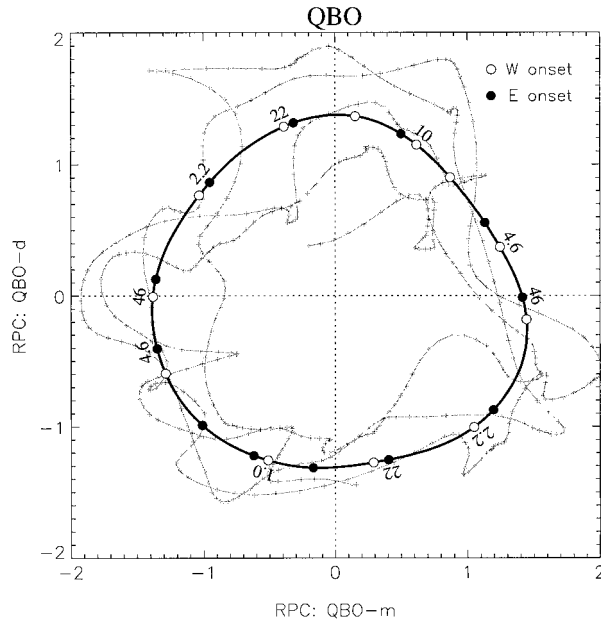


FIG. 12. Principal components of QBO modes from UKMO data. The corresponding EOF structures are shown in the companion paper (Dunkerton 2000). The thick curve provides a fit to the data, with westerly and easterly onset times indicated on the curve. The phase angle rotates counterclockwise with time.

related with anomalies of residual vertical velocity, since methane has a negative vertical gradient, and vertical velocity anomalies are anticorrelated with vertical shear of the mean zonal wind at the equator (Plumb and Bell 1982). Westerly shear zones are associated with relatively low methane concentration, and vice versa. For water vapor, an opposite relationship is obtained. The coincidence of vertical motion and tracer anomaly, instead of anomaly tendency, suggests that tracer anomalies are strongly damped at this altitude, perhaps by eddy mixing (Cordero et al. 1997; Randel et al. 1998) or photochemistry (S. Pawson 2000, personal communication).

For the two symmetric EOFs of ozone, the first leads the second, as shown by the symbol pattern. Positive values of the time series correspond to negative ozone anomalies near 22 and 31 hPa for the first and second symmetric EOFs, respectively. Maximum negative values at these altitudes are observed near a QBO phase of  $-\pi/2$  (Fig. 14h) and  $-\pi/4$  (Fig. 14i) coinciding approximately with easterly shear at 14 and 31 hPa, respectively (Fig. 12). The EOFs indicate that, at the same times, there is a negative anomaly in the upper stratosphere, located about 5 km below the altitude of westerly onset, suggesting that the temperature dependence of ozone cannot entirely explain this feature.

Interpretation of antisymmetric EOFs is more difficult, owing to their complicated spatial structure and peculiar time dependence. Two things should be kept in mind. First, when examining EOF structures it is wise to focus attention on the largest features rather than

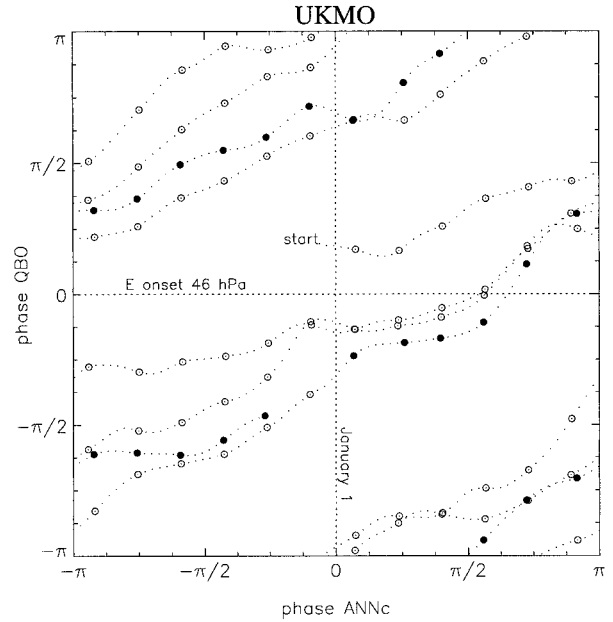


FIG. 13. Diagram showing the phase of the QBO vs the phase of the annual cycle defined by the calendar year ("ANNc"). Dots indicate pentads of UKMO low-pass filtered data. Circles indicate approximately the middle of each calendar month for which HALOE data are available. The first circle after "start" corresponds to Jan 1992. The last QBO cycle, with a period of 24 months, is indicated by solid circles.

attempting to interpret every detail. For methane and ozone (water vapor) first (second) antisymmetric EOF has its primary maximum in the northern subtropics just below 10 hPa. The other antisymmetric EOFs have their primary maxima in the southern subtropics near 4.6 hPa. It is mainly the variance at these locations that the rotated EOFs are trying to explain. Next in order of importance are features of opposite sign on the opposite side of the equator. The second antisymmetric EOF of water vapor lacks this feature, however. Second, concerning their time dependence, subbiennial variations should not be viewed in isolation from other modes. The seasonal dependence of QBO anomalies cannot be described by a single harmonic, whether quasi-biennial or subbiennial; rather, their superposition provides for the seasonality.

For seasonally adjusted methane, Fig. 8b suggests that in the middle stratosphere, negative anomalies in the northern subtropics coincide with QBO easterly onsets in the layer 10–31 hPa if such occur in northern spring or summer. This situation is realized in the first two QBO cycles (1993 and 1995), but in the third cycle (1997) the easterly onset occurs a little later<sup>2</sup> relative to the annual cycle, and the methane anomaly is split be-

<sup>2</sup> This delay can be reconciled with the seasonal synchronization of 46-hPa easterly onsets noting that the easterly descent was faster in the third cycle.

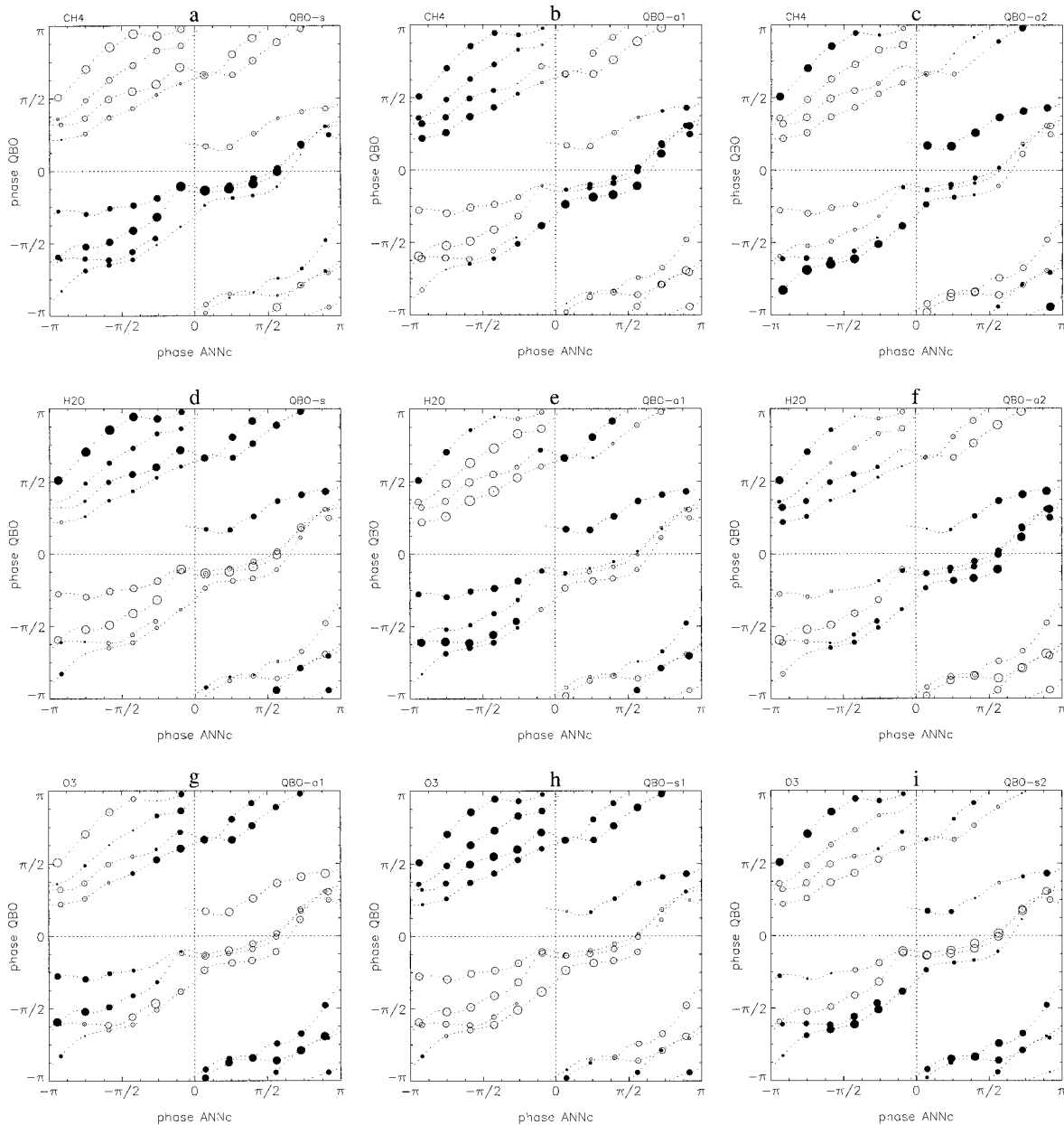


FIG. 14. Principal components of seasonally adjusted HALOE data displayed in the “phase diagram” format of Fig. 13. Symbol area is proportional to principal component value. Open (filled) circles denote positive (negative) values. Shown are the first three principal components of methane (a)–(c), water vapor (d)–(f), and ozone (g)–(i).

tween hemispheres. The anomaly south of the equator evidently prefers the southern spring season. This combination (of easterly QBO onset and southern spring) is realized in the third cycle more so than in the previous two.

Recent papers suggest that the QBO induced circulation is asymmetric at the solstices, with a stronger winter cell (Jones et al. 1998; Kinnersley 1999; L. J. Gray 1999, personal communication). Advection by the mean meridional circulation may create subtropical tracer anomalies during spring and summer opposite in sign

to those at the equator, as observed, if advection correlates with tracer *tendency* rather than with tracer itself. The pattern in Fig. 8b can be explained if easterly QBO onsets in the layer 10–31 hPa are accompanied by equatorial upwelling and subtropical subsidence during northern winter or spring, and by subsidence in southern spring. Similar reasoning applies to the subtropical water vapor anomaly, with change of sign. The equatorial water vapor anomaly, on the other hand, does not appear in methane and may be related to tape recorder variations.

Vertical transport does not entirely explain the subtropical anomaly, particularly of ozone, since the gradient of ozone is primarily horizontal near 10 hPa, yet ozone has the same subtropical anomaly as methane. Both tracers, in their time mean, have a negative latitudinal gradient in this region. If mean meridional advection is involved, negative anomalies in the subtropics could be due, in part, to equatorward flow of air from higher latitudes with low tracer concentration, and vice versa. By mass continuity, the equatorward branch of the QBO circulation cell is located at the base of the layer of equatorial upwelling in easterly shear. A somewhat larger role for meridional advection of ozone at 10 hPa, relative to vertical advection, may explain why subtropical ozone anomalies at this level are observed slightly ahead of the corresponding methane anomalies.

## 6. Conclusions

Interannual variability of trace constituents in the stratosphere was examined using methane, water vapor, and ozone data from the Halogen Occultation Experiment (HALOE) aboard the *Upper Atmosphere Research Satellite (UARS)* in 1992–99. Application of rotated principal component analysis to the dataset revealed dominant modes of variability consisting of annual, semiannual, and quasi-biennial oscillations (QBO), together with “subbiennial” variations evidently due to nonlinear interaction between the annual cycle and QBO. The structure of quasi-biennial variability is approximately symmetric about the equator, while subbiennial variability, with certain exceptions, is approximately antisymmetric and confined mostly to the subtropics. The semiannual variation of methane depends somewhat on the underlying QBO, implying a stronger “double peak” in the deep westerly phase. The vertical structure and downward propagation of the ozone QBO at the equator is described by a pair of symmetric EOFs having separate amplitude maxima in the lower and upper stratosphere. A second pair of EOFs explains the seasonal dependence of subtropical ozone anomalies. For each tracer, the subtropical anomaly is larger in the Northern Hemisphere. More years of data will be required in order to determine whether this asymmetry is a permanent feature, or the result of sampling during the *UARS* observing period in which only certain combinations of annual cycle and QBO have been realized.

A novel “phase diagram” illustrates the joint seasonal and QBO dependence of tracer anomalies. A pair of principal components were used to define the phase of the dynamical QBO. When plotted against the phase of the annual cycle, the QBO follows a diagonal trajectory with regular phase progression except for an occasional slowing of easterly shear-zone descent near 50 hPa. Tracer principal components of symmetric and antisymmetric EOFs, plotted along this trajectory, display the distinct signatures of quasi-biennial and subbiennial variation. Tracer anomalies reconstructed using an ideal-

ized representation of QBO and subbiennial harmonics display the seasonal synchronization and decadal modulation characteristic of QBO–annual cycle interaction. Using the harmonic time series extended over a full modulation cycle of 13 yr, and assuming a constant QBO period of 26 months, a climatology of anomaly variance was constructed for each tracer. These variance climatologies provide a quantitative measure of the magnitude and timing of seasonal synchronization.

The appearance of symmetric and antisymmetric EOFs, characterized by quasi-biennial and subbiennial variation in time, agrees with Hamilton’s (1995) spectral analysis of column ozone partitioned a priori into symmetric and antisymmetric components. In our case, subjective partitioning of data into symmetric and antisymmetric parts was unnecessary. For methane, the subbiennial component is approximately antisymmetric and confined mostly to the subtropics, suggesting that the annual variation of meridional transport, interacting with QBO anomalies, is important. While this mechanism is expected to influence water vapor in the similar way, we also found a significant, seasonally synchronized water vapor anomaly in the equatorial middle stratosphere. The symmetric part of the water vapor anomaly evidently contains a subbiennial harmonic in addition to its quasi-biennial harmonic; or equivalently, the subbiennial EOF overlaps the equator, and is asymmetric rather than antisymmetric. For ozone mixing ratio, credible evidence of seasonal synchronization was found in a small region north of the equator, in the middle stratosphere.

Additional constituent data from HALOE, which is ongoing, and from future EOS instruments will be valuable in several ways, determining with more certainty the fundamental EOF structures and underlying trends, while sampling many more combinations of the annual cycle and QBO. It will be interesting in the future to discover whether the results of our preliminary study are representative of a longer record. Given the overall similarity of HALOE tracers in the middle stratosphere and the much longer record of column ozone—both of which display seasonal variation in the subtropics with slow modulation in time—there is reason to be optimistic.

*Acknowledgments.* HALOE sounding data were obtained from Langley Research Center with the assistance of Anju Shah. Comments of Steve Pawson and two anonymous reviewers were helpful for the reorganization of this paper and its companion. This research was supported by the National Aeronautics and Space Administration, Contracts NAS1-96071, NAS1-99130, and NAS5-98078.

## REFERENCES

- Chipperfield, M. P., L. J. Gray, J. S. Kinnersley, and J. Zawodny, 1994: A two-dimensional model study of the QBO signal in SAGE II NO<sub>2</sub> and O<sub>3</sub>. *Geophys. Res. Lett.*, **21**, 589–592.

- Cordero, E. C., S. R. Kawa, and M. R. Schoeberl, 1997: An analysis of tropical transport: Influence of the quasi-biennial oscillation. *J. Geophys. Res.*, **102**, 16 453–16 461.
- Delisi, D. P., and T. J. Dunkerton, 1988: Seasonal variation of the semiannual oscillation. *J. Atmos. Sci.*, **45**, 2772–2787.
- Dunkerton, T. J., 1990: Annual variation of deseasonalized mean flow acceleration in the equatorial lower stratosphere. *J. Meteor. Soc. Japan*, **68**, 499–508.
- , 1991: Nonlinear propagation of zonal winds in an atmosphere with Newtonian cooling and equatorial wavelike driving. *J. Atmos. Sci.*, **48**, 236–263.
- , 2000: Midwinter deceleration of the subtropical mesospheric jet and interannual variability of the high-latitude flow in UKMO analyses. *J. Atmos. Sci.*, **57**, 3838–3855.
- , and D. J. O’Sullivan, 1996: Mixing zone in the tropical stratosphere above 10 mb. *Geophys. Res. Lett.*, **23**, 2497–2500.
- , and D. P. Delisi, 1997: Interaction of the quasi-biennial oscillation and stratospheric semiannual oscillation. *J. Geophys. Res.*, **102**, 26 107–26 116.
- Evans, S. J., R. Toumi, J. E. Harries, M. P. Chipperfield, and J. M. Russell III, 1998: Trends in stratospheric humidity and the sensitivity of ozone to these trends. *J. Geophys. Res.*, **103**, 8715–8725.
- Gray, L. J., and J. A. Pyle, 1986: The semiannual oscillation and equatorial tracer distributions. *Quart. J. Roy. Meteor. Soc.*, **112**, 387–407.
- , and T. J. Dunkerton, 1990: The role of the seasonal cycle in the quasi-biennial oscillation of ozone. *J. Atmos. Sci.*, **47**, 2429–2451.
- , and J. M. Russell III, 1999: Interannual variability of trace gases in the subtropical winter stratosphere. *J. Atmos. Sci.*, **56**, 977–993.
- Hamilton, K., 1989: Interhemispheric asymmetry and annual synchronization of the ozone quasi-biennial oscillation. *J. Atmos. Sci.*, **46**, 1019–1025.
- , 1995: Comment on “Global QBO in circulation and ozone. Part I: Reexamination of observational evidence.” *J. Atmos. Sci.*, **52**, 1834–1838.
- Hasebe, F., 1984: The global structure of the total ozone fluctuations observed on the time scales of two to several years. *Dynamics of the Middle Atmosphere*, J. R. Holton and T. Matsuno, Eds., Terra Scientific, 445–464.
- Hilsenrath, E., and B. M. Schlessinger, 1981: Total ozone seasonal and interannual variations derived from the 7-year Nimbus 4 BUV data set. *J. Geophys. Res.*, **86**, 12 087–12 096.
- Holton, J. R., 1989: Influence of the annual cycle in meridional transport on the quasi-biennial oscillation in total ozone. *J. Atmos. Sci.*, **46**, 1434–1439.
- , and W.-K. Choi, 1988: Transport circulation deduced from SAMS trace species data. *J. Atmos. Sci.*, **45**, 1929–1939.
- Jackson, D. R., M. D. Burrage, J. E. Harries, L. J. Gray, and J. M. Russell III, 1998: The semiannual oscillation in upper stratospheric and mesospheric water vapour as observed by HALOE. *Quart. J. Roy. Meteor. Soc.*, **124**, 2493–2515.
- Jones, D. B. A., H. R. Schneider, and M. B. McElroy, 1998: Effects of the quasi-biennial oscillation on the zonally averaged transport of tracers. *J. Geophys. Res.*, **103**, 11 235–11 249.
- Jones, R. L., and J. A. Pyle, 1984: Observations of CH<sub>4</sub> and N<sub>2</sub>O by the Nimbus 7 SAMS: A comparison with in situ data and two-dimensional numerical model calculations. *J. Geophys. Res.*, **89**, 5263–5279.
- Kennaugh, R., S. Ruth, and L. J. Gray, 1997: Modeling quasi-biennial variability in the semiannual double peak. *J. Geophys. Res.*, **102**, 16 169–16 187.
- King, J. C., W. H. Brune, D. W. Tooney, J. M. Rodriguez, W. L. Starr, and J. F. Vedder, 1991: Measurements of ClO and O<sub>3</sub> from 21°N to 61° in the lower stratosphere during February 1988: Implications for heterogeneous chemistry. *Geophys. Res. Lett.*, **18**, 2273–2276.
- Kinnersley, J. S., 1999: Seasonal asymmetry of the low- and middle-latitude QBO circulation anomaly. *J. Atmos. Sci.*, **56**, 1140–1153.
- Lait, L. R., M. R. Schoeberl, and P. A. Newman, 1989: Quasi-biennial modulation of the Antarctic ozone depletion. *J. Geophys. Res.*, **94**, 11 559–11 571.
- Leovy, C. B., C.-R. Sun, M. H. Hitchman, E. E. Remsberg, J. M. Russell III, L. L. Gordley, J. C. Gille, and L. V. Lyjak, 1985: Transport of ozone in the middle stratosphere: Evidence for planetary wave breaking. *J. Atmos. Sci.*, **42**, 230–244.
- Luo, M., J. M. Russell III, and T. Y. W. Huang, 1997: Halogen Occultation Experiment observations of the quasi-biennial oscillation and the effects of Pinatubo aerosols in the tropical stratosphere. *J. Geophys. Res.*, **102**, 19 187–19 198.
- Mote, P. W., and Coauthors, 1996: An atmospheric tape recorder: The imprint of tropical tropopause temperatures on stratospheric water vapor. *J. Geophys. Res.*, **101**, 3989–4006.
- , T. J. Dunkerton, M. E. McIntyre, E. A. Ray, P. H. Haynes, and J. M. Russell III, 1998: Vertical velocity, vertical diffusion, and dilution by midlatitude air in the tropical lower stratosphere. *J. Geophys. Res.*, **103**, 8651–8666.
- Murphy, D. M., D. W. Fahey, M. H. Proffitt, S. C. Liu, K. R. Chan, C. S. Eubank, S. R. Kawa, and K. K. Kelly, 1993: Reactive nitrogen and its correlation with ozone in the lower stratosphere and upper troposphere. *J. Geophys. Res.*, **98**, 8751–8773.
- Naujokat, B., 1986: An update of the observed quasi-biennial oscillation of the stratospheric winds over the tropics. *J. Atmos. Sci.*, **43**, 1873–1877.
- Nedoluha, G. E., R. M. Bevilacqua, R. M. Gomez, D. E. Siskind, B. C. Hicks, J. M. Russell III, and B. J. Connor, 1998a: Increases in middle atmosphere water vapor as observed by the Halogen Occultation Experiment and the ground-based Water Vapor Millimeter-wave Spectrometer from 1991 to 1997. *J. Geophys. Res.*, **103**, 3531–3543.
- , D. E. Siskind, J. T. Bacmeister, R. M. Bevilacqua, and J. M. Russell III, 1998b: Changes in upper stratospheric CH<sub>4</sub> and NO<sub>2</sub> as measured by HALOE and implications for changes in transport. *Geophys. Res. Lett.*, **25**, 987–990.
- Oort, A. H., 1983: *Global Atmospheric Circulation Statistics, 1958–1973*. NOAA Professional Paper 14, U.S. Govt. Printing Office, 180 pp.
- Plumb, R. A., and R. C. Bell, 1982: A model of the quasi-biennial oscillation on an equatorial beta-plane. *Quart. J. Roy. Meteor. Soc.*, **108**, 335–352.
- Politowicz, P. A., and M. H. Hitchman, 1997: Exploring the effects of forcing quasi-biennial oscillations in a two-dimensional model. *J. Geophys. Res.*, **102**, 16 481–16 497.
- Randel, W. J., and J. B. Cobb, 1994: Coherent variations of monthly mean total ozone and lower stratospheric temperature. *J. Geophys. Res.*, **99**, 5433–5447.
- , and F. Wu, 1996: Isolation of the ozone QBO in SAGE II data by singular value decomposition. *J. Atmos. Sci.*, **53**, 2546–2559.
- , B. A. Boville, J. C. Gille, P. L. Bailey, S. T. Massie, J. B. Kumer, J. L. Mergenthaler, and A. E. Roche, 1994: Simulation of stratospheric N<sub>2</sub>O in the NCAR CCM2: Comparison with CLAES data and global budget analyses. *J. Atmos. Sci.*, **51**, 2834–2845.
- , F. Wu, J. M. Russell III, A. Roche, and J. W. Waters, 1998: Seasonal cycles and QBO variations in stratospheric CH<sub>4</sub> and H<sub>2</sub>O observed in UARS HALOE data. *J. Atmos. Sci.*, **55**, 163–185.
- , —, —, and J. Waters, 1999a: Space-time patterns of trends in stratospheric constituents derived from UARS measurements. *J. Geophys. Res.*, **104**, 3711–3727.
- , —, R. Swinbank, J. Nash, and A. O’Neill, 1999b: Global QBO circulation derived from UKMO stratospheric analyses. *J. Atmos. Sci.*, **56**, 457–474.
- Reber, C. A., C. E. Trevathan, R. J. McNeal, and M. R. Luther, 1993: The Upper Atmosphere Research Satellite (UARS) mission. *J. Geophys. Res.*, **98**, 10 643–10 647.
- Rosenlof, K. H., A. F. Tuck, K. K. Kelly, J. M. Russell III, and M.

- P. McCormick, 1997: Hemispheric asymmetries in water vapor and inferences about transport in the lower stratosphere. *J. Geophys. Res.*, **102**, 13 213–13 234.
- Russell, J. M., III., and Coauthors, 1993: The Halogen Occultation Experiment. *J. Geophys. Res.*, **98**, 10 777–10 797.
- Ruth, S., R. Kennaugh, L. J. Gray, and J. M. Russell III, 1997: Seasonal, semiannual, and interannual variability seen in measurements of methane made by the UARS Halogen Occultation Experiment. *J. Geophys. Res.*, **102**, 16 189–16 199.
- Siskind, D. E., L. Froidevaux, J. M. Russell, and J. Lean, 1998: Implications of upper stratospheric trace constituent changes observed by HALOE for O<sub>3</sub> and ClO from 1992 to 1995. *Geophys. Res. Lett.*, **25**, 3513–3516.
- Solomon, S., J. T. Kiehl, R. R. Garcia, and W. Grose, 1986: Tracer transport by the diabatic circulation deduced from satellite observations. *J. Atmos. Sci.*, **43**, 1603–1617.
- Stanford, J. L., J. R. Ziemke, and S. Y. Gao, 1993: Stratospheric circulation features deduced from SAMS constituent data. *J. Atmos. Sci.*, **50**, 226–246.
- Sun, C.-R., and C. B. Leovy, 1990: Ozone variability in the equatorial middle atmosphere. *J. Geophys. Res.*, **95**, 13 829–13 849.
- Trepte, C. R., and M. H. Hitchman, 1992: The stratospheric tropical circulation deduced from aerosol satellite data. *Nature*, **355**, 626–628.
- Tung, K. K., and H. Yang, 1994: Global QBO in circulation and ozone. Part I: Reexamination of observational evidence. *J. Atmos. Sci.*, **51**, 2699–2707.
- Wallace, J. M., R. L. Panetta, and J. Estberg, 1993: Representation of the equatorial stratospheric quasi-biennial oscillation in EOF phase space. *J. Atmos. Sci.*, **50**, 1751–1762.
- Zawodny, J. M., and M. P. McCormick, 1991: Stratospheric Aerosol and Gas Experiment II measurements of the quasi-biennial oscillations in ozone and nitrogen dioxide. *J. Geophys. Res.*, **96**, 9371–9377.